SCIENTIFIC REPORTS
nature research

OPEN

Microstructure and superconducting properties of high-rate PLD-derived $GdBa_2Cu_3O_{7-\delta}$ coated conductors with $BaSnO_3$ and $BaZrO_3$ pinning centers

Alexey V. Ovcharov[1], Pavel N. Degtyarenko[2,3], Vsevolod N. Chepikov[2,4], Alexander L. Vasiliev[1,5,6*], Sergey Yu. Gavrilkin[7], Igor A. Karateev[1], Alexey Yu. Tsvetkov[7] & Andrey R. Kaul[2,4]

The microstructure of $GdBa_2Cu_3O_{7-\delta}$ based on superconducting tapes with $BaSnO_3$ and $BaZrO_3$ artificial pinning centers formed by high-rate pulse laser deposition in SuperOx Japan was studied by scanning/transmission electron microscopy. The artificial pinning centers have adopted columnar morphology with average diameter of about 8 nm ($BaSnO_3$-doped sample) and 6.5 nm ($BaZrO_3$-doped sample) and density of 500 μm^{-2} for the both samples. The average length of the $BaSnO_3$ nanocolumns is about two times higher than the $BaZrO_3$ nanocolumns. The angular dependences of critical current in magnetic field up to 1 Tesla at 77 and 65 K have been obtained. The critical current and its anisotropy depend on artificial pinning centers presence and their type. The angular dependence of resistivity in the field up to 9 Tesla was also studied and discussed.

The commercial production of second generation high temperature superconducting tapes (2G HTS tapes, coated conductors, CC) based on $REBa_2Cu_3O_{7-\delta}$ (where *RE* is a rare-earth element, *RE*BCO) is rapidly developing in many countries and that can be proved by large number of publications[1–4]. Various devices for power industry based on 2G HTS wires like power cables, fault current limiters, various types of motors and inductive drives etc. have already been designed and tested[5–7]. However, the improvement of CC's performance in magnetic field is still necessary and that is the goal of a number of investigations. The practice shows that intrinsic defects of CC's, like point defects, misfit dislocation, twin boundaries, grain boundaries, and other crystal lattice imperfections do not pin vortexes strong enough. One way to increase the in-field stability of CC's critical current density, j_c, at LN_2 temperatures is the introduction of artificial pining centers (APC). First APC's in superconducting films were obtained by nano-islands on substrate (substrate decoration) on Ti-base films[8]. The possibility to increase the j_c in $YBa_2Cu_3O_{7-\delta}$ CC's with APC was shown by MacManus-Driscoll and co-workers in 2004[9], later on the validity of this approach was demonstrated in a number of papers[10–13]. Introduction of the APC had increased the lift-factor and significantly reduced the critical current (I_c) anisotropy in strong magnetic fields (up to 10 Tesla) at $T \gg 77$ K. The lift-factor is the ratio of I_c at certain temperature and magnetic field value to the I_c of the same sample at 77 K in self-field (s.f.) (lift-factor = I_c (77 K, 1 T, Θ)/I_c(77 K, s.f.)). SuperOx company also started the R&D program oriented on high-rate manufacturing of CC's with perovskite APC[14,15]. It is important to understand the contribution of APCs to the final pinning force value and its dependence on temperature and external magnetic field, including its orientation[16,17]. To solve this problem one have to determine the microstructural characteristics of HTS tapes with a different type of APC. In present study, we compared commercial CC's, 12 mm wide, without APC (REF

[1]National Research Center "Kurchatov Institute", Moscow, 123182, Russia. [2]SuperOx, Moscow, 117246, Russia. [3]Joint Institute for High Temperature of Russian Academy of Sciences, Moscow, 125412, Russia. [4]Lomonosov Moscow State University, Moscow, 119991, Russia. [5]Shubnikov Institute of Crystallography of Russian Academy of Sciences, Moscow, 117333, Russia. [6]Moscow Institute of Physics and Technology (State University), Dolgoprudny, Moscow Region, 141701, Russia. [7]P.N. Lebedev Physical Institute of the Russian Academy of Sciences, Moscow, 119991, Russia. *email: a.vasiliev56@gmail.com

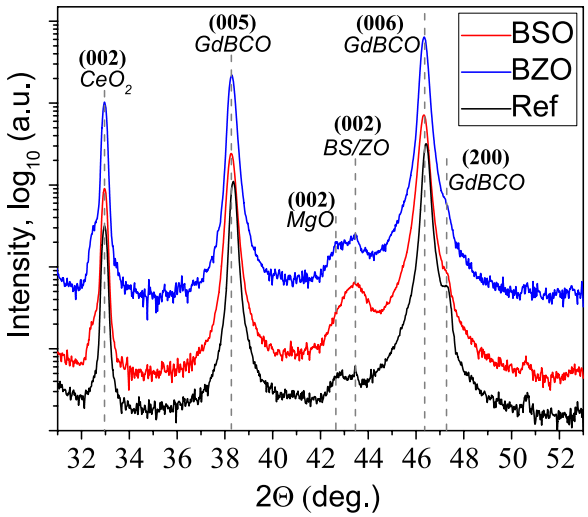

Figure 1. XRD data of the 2G HTS tapes.

sample) and those obtained at the same high rate pulse laser deposition (PLD) of GdBCO layer doped with 6 molar % $BaSnO_3$ (BSO sample) and $BaZrO_3$ (BZO sample) APC. The correlation of CC's microstructure studied by transmission electron microscopy (TEM) and their superconducting characteristics was also considered.

Results

Phase composition, texture and microstructure of samples. The X-Rays diffraction (XRD) data are shown in Fig. 1. The HTS layer and the CeO_2 top buffer layer have texture with predominant (001) orientations. For the REF sample and BSO sample there is a small amount of (100) oriented grains (*a*-orientation) in the HTSC layer, which is positioned as the right shoulder of (006) GdBCO peak in the XRD scans. Two low-intensity peaks around 44° on the XRD scans of the REF sample correspond to (002) reflection of the MgO buffer layer and (111) reflection of Hastelloy (Ni-based alloy) substrate. More intensive (002) BSO and BZO reflections are also located in this area of the XRD pattern, overlapping with MgO (002) and Ni (111) reflections of the doped samples. Other reflections of APC were not detected and that referred to the texture of APC particles with orientational relationship between APC and HTS as - (001) BSO/BZO||(001) $GdBa_2Cu_3O_{7-\delta}$.

Bright Field (BF) TEM cross-section overall images of all samples are shown in supplementary Fig. S1. These images demonstrate that the BSO and BZO adopted nanocolumn morphology, with the elongation towards the growth direction of GdBCO layer. The enlarged images of the samples (Fig. 2) demonstrate specific moiré patterns associated with the APC nanocolumns, which arose from the overlay of the APC and HTS matrix crystal lattices. Based on such images the average diameter of nanocolumns and APC density values were calculated and the results are presented in Table 1. We found that the nanocolumns are slightly tilted in relation to the GdBCO *c*-axis. The average tilt angles of the nanocolumns have ≈4.5° and ≈11° for BSO and BZO samples, respectively. The mismatch between the BSO (BZO) and GdBCO crystal lattices can be partly released due to the formation of partial dislocations with the projection of Burgers vector parallel to 110 GdBCO crystal planes, but not to 100 or 010 crystal planes and this is visible on the Fourier filtered images of selected area (Fig. 3 and supplementary Fig. S2). The "1-2-4" plane defects were observed in all the samples and these defects could influence the superconducting properties[16].

Figure 4 shows TEM images of the plan-view samples. The nanocolumns density and their average diameter were determined in these images and the results are presented in Table 1.

Superconducting properties. The T_c and I_c values of the samples (77 K, s.f.) are presented in Table 1. The angle dependences of critical current for all the samples are presented in Fig. 5. The I_c at 77 K in REF sample is higher than in other samples for all field orientations and I_c in turn is higher in the BSO sample than in BZO sample.

At 65 K the difference of critical currents between reference and doped samples becomes lower. For the field orientation B||c the I_c values in reference and doped samples become smaller, and I_c is still higher in BSO sample. The lift-factor in the samples with APC is higher at 77 K comparing to REF sample for all field orientations and it reaches the highest value at 65 K. At this temperature and field value of 1 T the angular dependence becomes more isotropic.

The temperature dependence of the resistivity. The APC introduction resulted in the decrease of T_c. The T_c for the REF sample is 93 K. The T_c for the BSO sample and BZO sample are 91.9 K and 91 K, correspondingly (supplementary Fig. S3). The T_c decreases in high magnetic field and the transition broads to few Kelvins in all samples. The infield broadening in BZO sample is less than in REF sample. The larger T_c decrease was observed, when the field orientation was changed from **B**||*ab* to **B**||*c*.

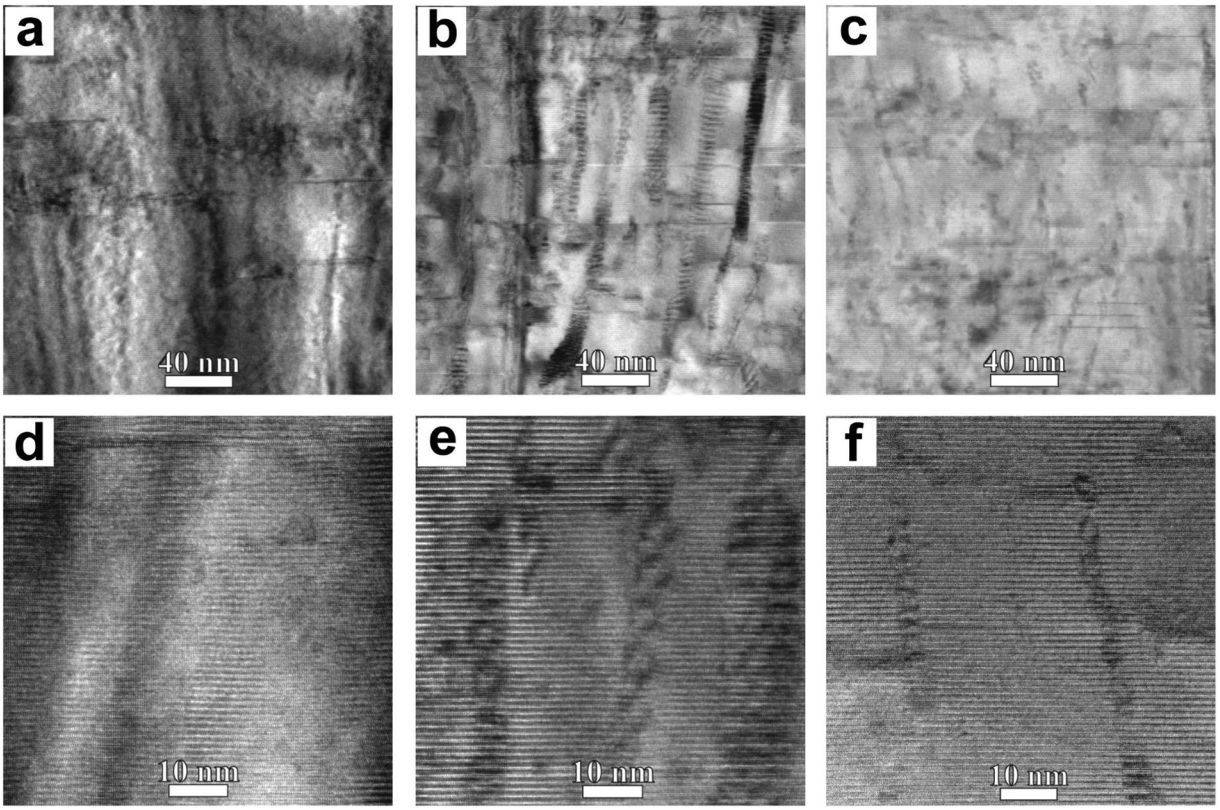

Figure 2. Enlarged TEM cross-section images with different magnifications: (**a**,**d**) reference sample, (**b**,**e**) BSO sample, (**c**,**f**) BZO sample. Enlarged images demonstrates visible APC nanocolumns.

APC dopant		Undoped sample	$BaSnO_3$ sample	$BaZrO_3$ sample
T_c		93.3	91.9	91.0
I_c at 77 K (A/12 mm)		360	140	120
Density of APC	plan-view estimates (μm^{-2})	—	400 ± 100	500 ± 100
	cross-section estimates (μm^{-2})	—	600 ± 200	600 ± 200
cmAverage diameter of the nanocolumns	plan-view estimates (nm)	—	7.9 ± 3.3	7.1 ± 2.9
	cross-section estimates (nm)	—	8.5 ± 2.2	6.3 ± 1.3

Table 1. Electophysical and microstructural characteristics of the 2G HTS tape samples with APC and reference sample.

The logarithmic of resistivity (In*R*) versus 1/T dependencies are shown in Fig. 6. The In*R* in the REF sample looks differently from the doped samples, with a kink and two ranges of different slopes. At high magnetic field the kink is more evident.

Discussion

The microstructural analysis of 2 G HTS tapes demonstrates that the BSO and BZO nanocolumns are formed in the doped samples with the typical diameter of ≈8 nm and ≈6.5 nm, respectively. These values are in close correlation with ones found in the previous study[13]. We found that the APCs in both types of samples are not strictly parallel to [001] GdBCO, but were tilted up to 24° (see Fig. 2). Similar results presented in the study of Maeda *et al.*[18] for $BaHfO_3$ embedded in GdBCO matrix. The angular dependence of the nanocolumns on the substrate temperature and growth rate were discussed by Ichino *et al.*[19]. The APC insertion leads to a drop of T_c. The authors of next article indicated that T_c is influenced by uniaxial stress and we suppose that the strains at the B(S/Z)O/GdBCO interface could cause the change of T_c[20]. The cooling down to 65 K increases the critical current value and lift-factor in comparison with the critical current value and lift-factor at 77 K and also decreases its anisotropy under the external magnetic field, this is clearly observed in the angular dependencies of the critical current in the magnetic fields up to 1 T. These data demonstrate the efficiency of APC. The I_c values and the lift-factor increase even more with further decrease of temperature and further increase of the external fields up to 9 T, which was demonstrated in our previous publications[14,15].

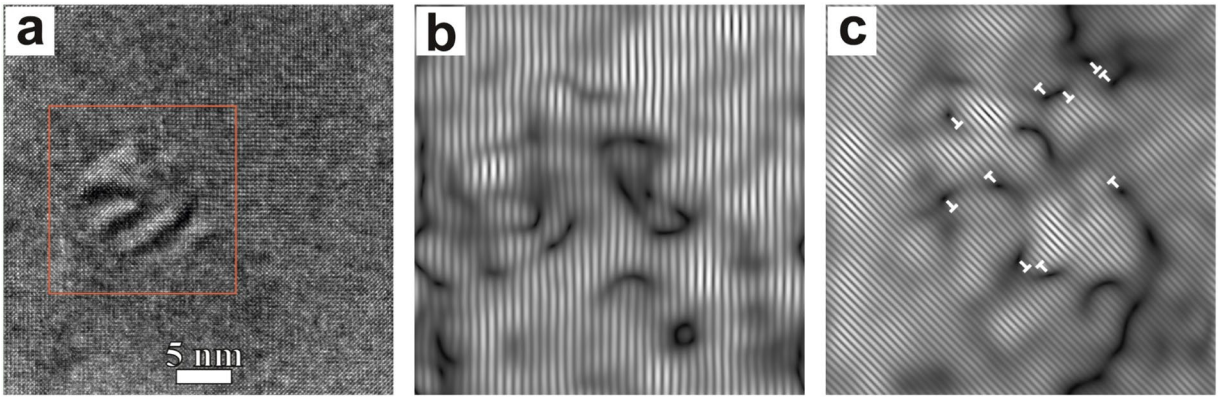

Figure 3. (**a**) HR TEM plan-view image BSO sample and the Fourier filtered images of selected area marked by red square and obtained from the reflexes: (**b**) $0\bar{1}0_{GdVCO}$ and 100_{BSO}, (**c**) $1\bar{1}0_{GdBCO}$ and 110_{BSO}. Extra crystal planes are marked by ⊥.

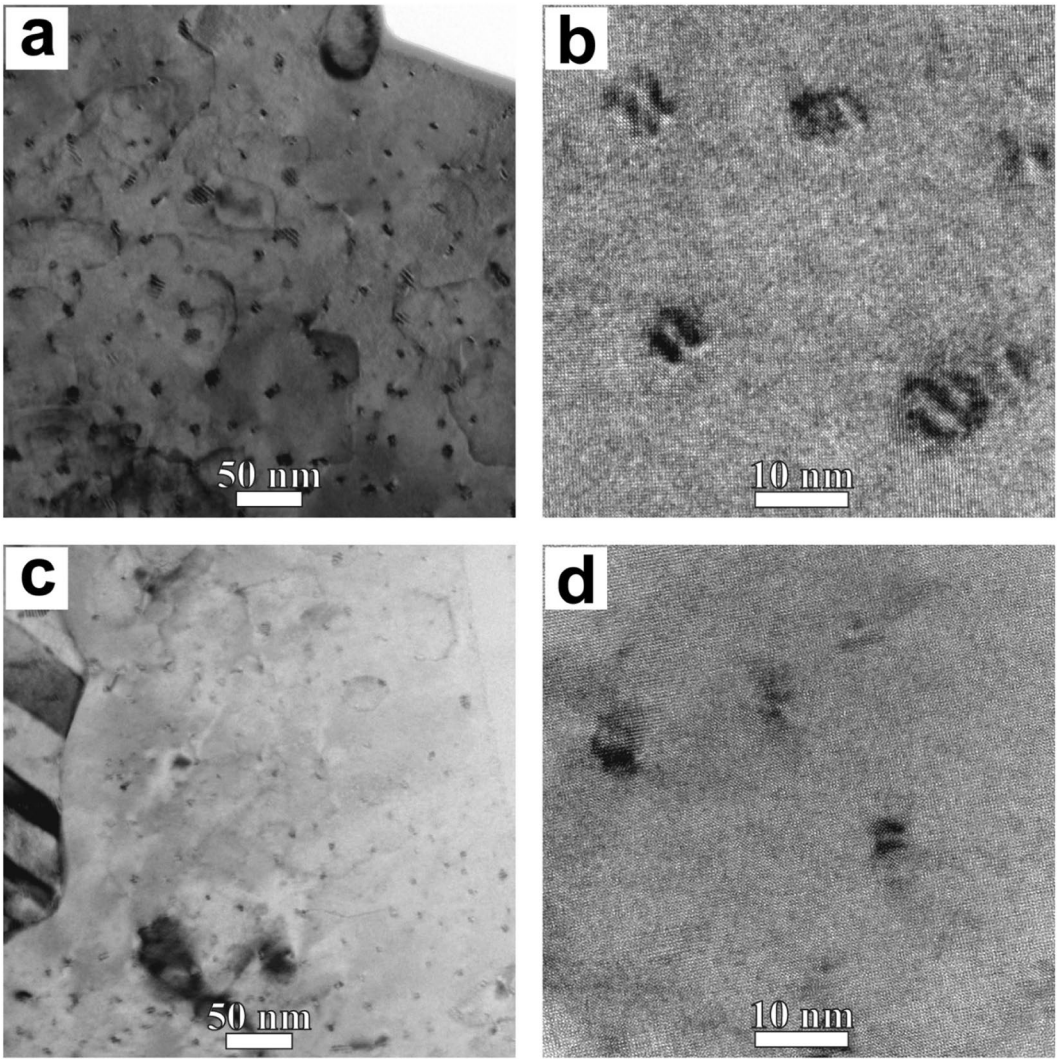

Figure 4. TEM plan-view images with different magnifications (**a**), (**b**) BSO sample; (**c**), (**d**) BZO sample.

External magnetic field shifts down and enlarge the temperature range of transition to superconducting state. The InR vs 1/T graphs reveal two ranges of different slopes in the vicinity of T_c, the difference is more expressed when the field is increased up to 9 T (Fig. 6). The observation is accompanied by the fact that the magnetic field

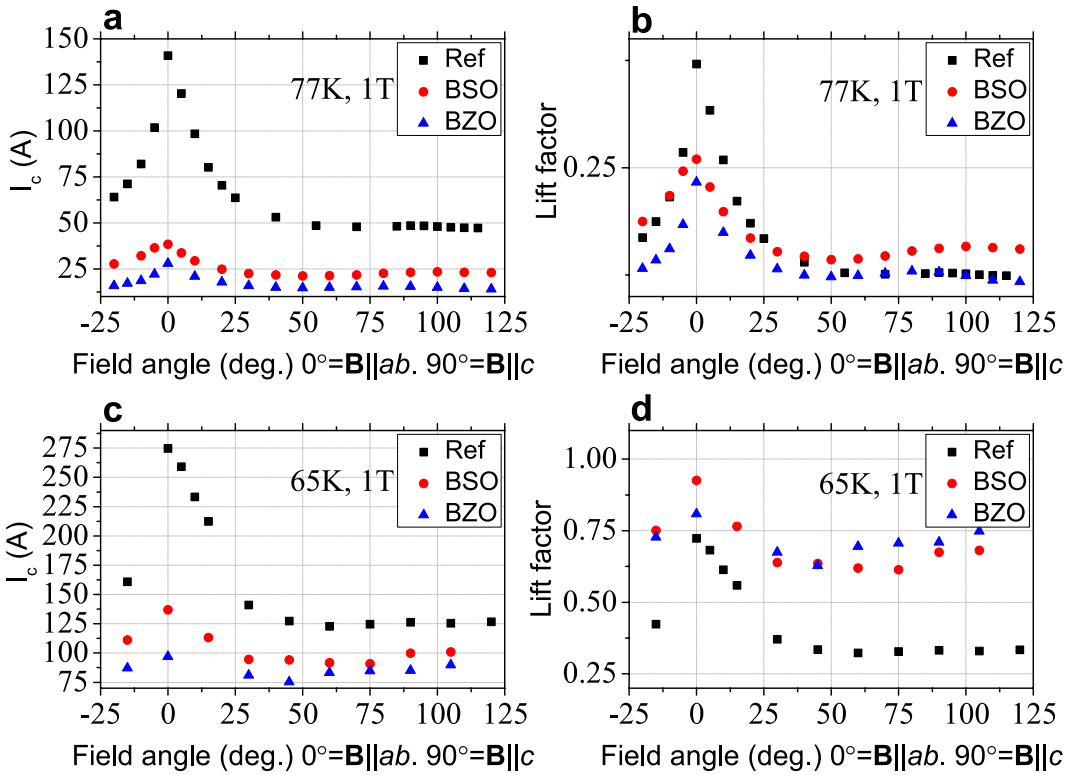

Figure 5. Angular dependence of absolute I_c value (**a**,**c**) and lift-factor (**b**,**d**) at applied magnetic field 1 Tesla, 77 K and 65 K.

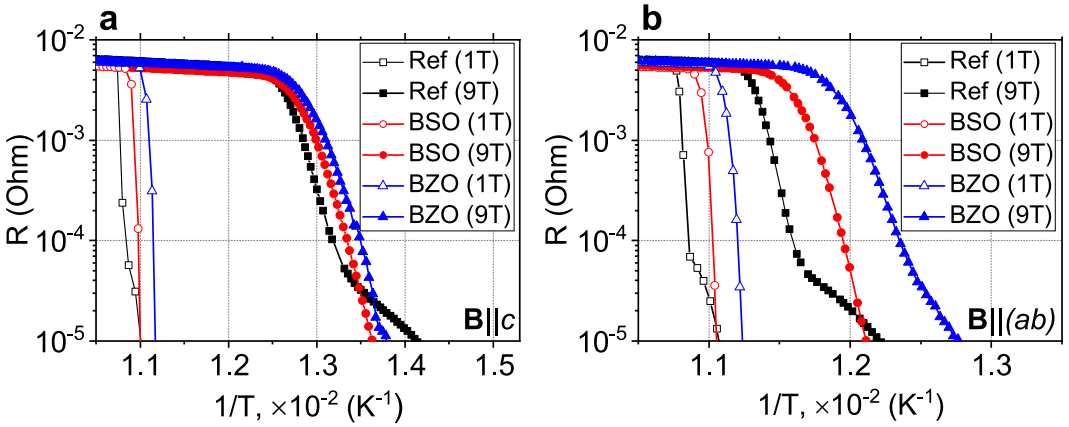

Figure 6. Dependence of InR versus 1/T for all samples in the field (**a**) **B**||c and (**b**) **B**||(ab).

influenced differently on the samples when it was turned from **B**||c to **B**||(ab). These results indicate together that two types of pinning centers exist in the REF GdBCO sample which can be nanoparticles Gd_2O_3 and planar defects containing extra copper oxide easy detectable by TEM. This conclusion correlates also with the results presented in recent publication[21]. In the field **B**||(ab), evidently, the planar defects are mostly effective. In the sample with the APC, the predominant contribution of transverse type defects can be explained by the fact that the APC size is larger than the size of the plane defects and comparable to the size of the vortexes. Thus vortexes pin preferably on these APC defects.

The external magnetic field reduces the activation energy for all types of samples. For the REF sample and the BSO sample, the activation energy in the 1 T field **B**||c is of ≈0.95 eV, and for the BZO sample is of 0.86 eV. In the field **B**||(ab), the activation energy for all types of samples increases slightly as compared with the case, when **B**||c. As the external magnetic field increases, the activation energy also increases. It is worth noting that the rotation of the external magnetic field leads to a decrease in the activation energy for all samples. This decrease is larger for the REF and BSO samples.

The close inspection of cross-section images of whole HTS layers shows that APC average length (L_a) of the nanocolumns in the BSO sample is described by a log-normal distribution log $N(\mu, \sigma^2)$ with parameters $\mu = 4.56$ and $\sigma = 0.48$. The L_a value (determines as expectation) is 107.1 nm. For the BZO sample the log $N(\mu, \sigma^2)$ distribution has the parameters $\mu = 3.67$ and $\sigma = 0.58$, the value of L_a is 46.5 nm. Thus, it was found, that L_a value of the nanocolumns is about twice larger in the BSO sample. There is a good match of these data with the field dependence of pinning force, (supplementary Fig. S4), and the results of recent study[22]. The authors of that study concluded that a higher value of current density corresponds to the longer mean length and a smaller average diameter of the APC. The value of the pinning force for our BSO sample and BZO sample are 32.1 $N \cdot m^{-3}$ and 22.5 $N \cdot m^{-3}$, respectively. We followed the postulates of the authors[22] for the estimation of the pinning energy: $U = L_a \times u_0$ and authors[23] for the calculation of pinning energy per unit length: $u_o = \frac{1}{2}\varepsilon_0 \, ln\left(1 + \left(\frac{C_0}{\sqrt{2}\,\xi_{ab}}\right)^2\right)$, where: $\varepsilon_0 = (\Phi_0/4\pi\,\lambda_{ab})^2$, C_0 — radius of APC, Φ_0 — flux quantum, $\lambda_{ab} = \lambda_0\,(1 - t^4)^{-0.5}$ and $\xi_{ab} = \xi_0\,(1 - t)^{-0.5}$, where $t = T/T_c$. Taking into account the mean length estimated by the TEM, the pinning energy for BSO sample and BZO sample are $U = L_a \times u_0 = 0.85 \times 10^{-19}\,J = 0.91$ eV and $U = L_a \times u_0 = 0.12 \times 10^{-19} J = 0.59$ eV, correspondingly. The difference between these values is ≈1.6 times due to the larger average length of the APC in BSO sample. In this sample, the nanocolumns produce more valued effect on the anisotropy reduction and do not suppress strongly T_c value in comparison with the REF sample.

Methods

The GdBCO layers on IBAD MgO substrates with CeO_2 terminating layer were formed by PLD in reel-to-reel regime with layer growth rate of 750 $nm \cdot min^{-1}$, which is typical for the pilot-scale equipment at SuperOx. The samples preparation in more details was described in[14,15]. The schematic representation of the sample microstructure is shown in supplementary Fig. S5.

The XRD was performed in parallel beam geometry in a 5-circle Rigaku SmartLab diffractometer (Rigaku Corp., Japan) equipped with a 9 kW X-ray source with rotating copper anode. $2\Theta/\omega$-scan was performed for the phase analysis and ω- and j-scans aimed texture sharpness analysis.

TEM studies were performed on a S/TEM Titan 80–300 (Thermo Fisher Scientific, USA) equipped with a spherical aberration probe corrector, an energy dispersive X-ray spectrometer (EDAX, USA) and high angle annular dark field detector (Fischione, USA). The microscope was operated at 300 kV. The JEMS software developed by P. Stadelman was used for electron diffraction patterns and image simulations[24]. Cross-sectional samples were prepared using a focused Ga^+ ion beam in a scanning electron microscope (FIB/SEMs) Helios Nanolab 600i (Thermo Fisher Scientific, USA) equipped with a Pt, W gas injection systems (GIS) and an Omniprobe 200 micromanipulator (Omniprobe, USA). To obtain planar-sections of the samples, a FIB/SEMs Versa 3D DualBeam (Thermo Fisher Scientific, USA), equipped with a Pt and W GIS, and an EasyLift micromanipulator (Thermo Fisher Scientific, USA) was used in high vacuum mode.

Angular dependences of the I_c at 65 and 77 K in the fields up to 1 T were measured by four-probe technique described in[17]. Other electrophysical measurements and the temperature dependence of the resistivity were carried out using PPMS-9 (Quantum design, USA). The following experiment parameters were used in the four-probe measurements: the distance between the contacts was of 6.5 mm and DC-current — 100 mA. The magnetic field was varied between 0 and 9 T (with exact values 0.1, 0.3, 1, 3, and 9 T).

Received: 8 April 2019; Accepted: 19 September 2019;
Published online: 23 October 2019

References

1. Sundaram, A. *et al.* 2G HTS wires made on 30 mm thick Hastelloy substrate. *Supercond. Sci. Technol.* **29**, 104007, https://doi.org/10.1088/0953-2048/29/10/104007 (2016).
2. Usoskin, A., Betz, U., Dietrich, R. & Schlenga, K. Long HTS coated conductors processed via large area PLD/ABAD deposition for high field applications. *IEEE Transactions on Appl. Supercond.* **26**, 1–4, https://doi.org/10.1109/TASC.2016.2542253 (2016).
3. Lee, S. *et al.* Development and production of second generation high T_c superconducting tapes at SuperOx and first tests of model cables. *Supercond. Sci. Technol.* **27**, 044022, https://doi.org/10.1088/0953-2048/27/4/044022 (2014).
4. Izumi, T. Achievements in M-PACC project and future prospects on R&D of coated conductors in Japan. *Phys. Procedia* **58**, 6–9, https://doi.org/10.1016/j.phpro.2014.09.002 (2014).
5. Ruiz, H. S., Zhang, X. & Coombs, T. Resistive-type superconducting fault current limiters: concepts, materials, and numerical modeling. *IEEE Transactions on Appl. Supercond.* **25**, 1–5, https://doi.org/10.1109/TASC.2014.2387115 (2015).
6. Lee, S. J. *et al.* Recent status and progress on HTS cables for AC and DC power transmission in Korea. IEEE Transactions on. *Appl. Supercond.* **28**, 1–5, https://doi.org/10.1109/TASC.2018.2820721 (2018).
7. Larbalestier, D., Gurevich, A., Feldmann, D. M. & Polyanskii, A. High-T_c superconducting materials for electric power applications. In Dusastre, V. (ed.) *Materials For Sustainable Energy: A Collection of Peer-Reviewed Research and Review Articles from Nature Publishing Group*, 311–320, https://doi.org/10.1142/9789814317665_0046 (Co-Published with Macmillan Publishers Ltd, UK, 2010).
8. Crisan, A., Fujiwara, S., Nie, J., Sundaresan, A. & Ihara, H. Sputtered nanodots:A costless method for inducing effective pinning centers in superconducting thin films. *Appl. physics letters* **79**, 4547–4549, https://doi.org/10.1063/1.1428632 (2001).
9. MacManus-Driscoll, J. *et al.* Strongly enhanced current densities in superconducting coated conductors of $YBa_2Cu_3O_{7-x} + BaZrO_3$. Nat. *materials* **3**, 439–443, https://doi.org/10.1038/nmat1156 (2004).
10. Ionescu, M., Li, A., Zhao, Y., Liu, H. & Crisan, A. Enhancement of critical current density in $YBa_2Cu_3O_{7-\delta}$ thin films grown using PLD on YSZ (001) surface modified with Ag nano-dots. *J. Phys. D: Appl. Phys.* **37**, 1824–1828, https://doi.org/10.1088/0022-3727/37/13/014 (2004).
11. Schlesier, K., Huhtinen, H., Paturi, P., Stepanov, Y. P. & Laiho, R. Structural and superconducting properties of undoped and BZO-doped GdBCO thin films. IEEE Transactions on. *Appl. Supercond.* **19**, 3407–3411, https://doi.org/10.1109/TASC.2009.2017766 (2009).

12. Ko, K.-P. *et al*. Optimization of the $BaSnO_3$ doping content in $GdBa_2Cu_3O_{7-\delta}$ coated conductors by pulsed laser deposition. IEEE Transactions on. *Appl. Supercond.* **24**, 1–8, https://doi.org/10.1109/TASC.2014.2338296 (2014).
13. Tobita, H. *et al*. Fabrication of $BaHfO_3$ doped $Gd_1Ba_2Cu_3O_{7-\delta}$ coated conductors with the high I_c of 85 A/cm-w under 3 T at liquid nitrogen temperature (77 K). *Supercond. Sci. Technol.* **25**, 062002, https://doi.org/10.1088/0953-2048/25/6/062002 (2012).
14. Chepikov, V. *et al*. Introduction of $BaSnO_3$ and $BaZrO_3$ artificial pinning centres into 2G HTS wires based on PLDGdBCO films. phase I of the industrial R&D programme at SuperOx. *Supercond. Sci. Technol.* **30**, 124001, https://doi.org/10.1088/1361-6668/aa9412 (2017).
15. Chepikov, V. *et al*. Pinning properties of PLD-obtained $GdBa_2Cu_3O_{7-x}$ coated conductors doped with $BaSnO_3$. IEEE Transactions on. *Appl. Supercond.* **27**, 1–5, https://doi.org/10.1109/TASC.2017.2652323 (2017).
16. Feighan, J., Kursumovic, A. & MacManus-Driscoll, J. Materials design for artificial pinning centres in superconductor PLD coated conductors. *Supercond. Sci. Technol.* **30**, 123001, https://doi.org/10.1088/1361-6668/aa90d1 (2017).
17. Sychugov, V. V. *et al*. Variation of critical current and n-value of 2G HTS tapes in external magnetic fields of different orientation. In *Journal of Physics: Conference Series*, vol. 747, 012048, https://doi.org/10.1088/1742-6596/747/1/012048 (2016).
18. Maeda, T. *et al*. Nanostructural characterization of artificial pinning centers in PLD-processed $REBa_2Cu_3O_{7-x}$ films. *Ultramicroscopy* **176**, 151–160, https://doi.org/10.1016/j.ultramic.2016.11.015 (2017).
19. Ichino, Y., Yoshida, Y. & Miura, S. Three-dimensional Monte Carlo simulation of nanorod self-organization in $REBa_2Cu_3O_y$ thin films grown by vapor phase epitaxy. *Jpn. J. Appl. Phys.* **56**, 015601, https://doi.org/10.7567/JJAP.56.015601 (2016).
20. Crommie, M. *et al*. c-axis stress dependence of normal and superconducting state properties of $YBa_2Cu_3O_7$. *Phys. Rev. B* **39**, 4231, https://doi.org/10.1103/PhysRevB.39.4231 (1989).
21. Usoskin, A. *et al*. Double-disordered HTS-coated conductors and their assemblies aimed for ultra-high fields: large area tapes. IEEE Transactions on. *Appl. Supercond.* **28**, 1–6, https://doi.org/10.1109/TASC.2018.2801348 (2018).
22. Mele, P. *et al*. Ultra-high flux pinning properties of $BaMO_3$-doped $YBa_2Cu_3O_{7-x}$ thin films (M = Zr, Sn). *Supercond. Sci. Technol.* **21**, 032002, https://doi.org/10.1088/0953-2048/21/3/032002 (2008).
23. Nelson, D. R. & Vinokur, V. M. Boson localization and correlated pinning of superconducting vortex arrays. *Phys. Rev. B* **48**, 13060, https://doi.org/10.1103/PhysRevB.48.13060 (1993).
24. Stadelmann, P. EMS-a software package for electron diffraction analysis and HREM image simulation in materials science. *Ultramicroscopy* **21**, 131–145, https://doi.org/10.1016/0304-3991(87)90080-5 (1987).

Acknowledgements

The experimental part of this work was partially done with the equipment of the Resource Center of Probe and Electron Microscopy (Kurchatov Complex of NBICS-Technologies) NRC "Kurchatov Institute". The magnetic measurements were carried at LPI Shared Facility Centre for Studies of HTS and other Strongly Correlated Materials. The work was partly supported by Russian Foundation for Basic Researches, grant 17-0301298 and Ministry of Science and High Education within State assignment FSRC "Crystallography and Photonics" RAS.

Author contributions

A.L. and A.R. initiated the study; A.V., with the support I.A., performed the TEM and interpreted the results; P.N. analyzed and interpreted the results of measuring the superconducting properties of HTSC; A.V. and P.N. prepared the manuscript; V.N. prepared the samples of HTSC and performed XRD; S.Yu. carried out the measurements of temperature dependence of the resistivity in magnetic fields up to 9 T; A.Yu. carried out the measurements of angular dependence of I_c at applied magnetic field up to 1 T and T 77 K and 65 K. All authors discussed the results of the manuscript.

Competing interests

The authors declare no competing interests.

Additional information

Supplementary information is available for this paper at https://doi.org/10.1038/s41598-019-51348-w.

Correspondence and requests for materials should be addressed to A.L.V.

Reprints and permissions information is available at www.nature.com/reprints.

Publisher's note Springer Nature remains neutral with regard to jurisdictional claims in published maps and institutional affiliations.